Macromolecular Nanotechnology

HNBR and its MWCNT reinforced nanocomposites: Crystalline morphology and electrical response

CrossMark

G.C. Psarras [a],*, G.A. Sofos [a], A. Vradis [b], D.L. Anastassopoulos [b], S.N. Georga [b], C.A. Krontiras [b], J. Karger-Kocsis [c]

[a] *Department of Materials Science, University of Patras, Patras 26504, Greece*
[b] *Department of Physics, University of Patras, Patras 26504, Greece*
[c] *MTA–BME Research Group for Composite Science and Technology, Műegyetem rkp. 3., H-1111 Budapest, Hungary*

ARTICLE INFO

ABSTRACT

Morphology and electrical response of hydrogenated acrylonitrile butadiene rubber (HNBR) and its multiwall carbon nanotube (MWCNT) reinforced nanocomposites were studied by means of X-ray diffraction and broadband dielectric spectroscopy. HNBR systems were found to be semi-crystalline, with their crystallinity to increase with the addition of MWCNTs. In their dielectric spectra, four relaxation processes were detected. Ascending in relaxation time, these were attributed to: (i) interfacial polarization at the interface of crystalline and amorphous regions of HNBR and at the interface between HNBR and MWCNTs, (ii) glass to rubber transition of the amorphous part of HNBR, (iii) rearrangement of polar side groups, such as –CN, and (iv) local motions of small segments of the main elastomer chain.

Electrical conductivity increases with MWCNT content and frequency increment. The effect of temperature, on the electrical response, is more pronounced at low frequencies. The temperature dependence of the electrical conductivity strongly deviates from a pure Arrhenius behavior, signifying that the occurring conductance mechanisms do not correspond to a single thermally activated process. Relaxation dynamics imply that crystalline regions exert motion restrictions to large segments of the macromolecules in the amorphous phase and to polar parts of the systems.

© 2014 Elsevier Ltd. All rights reserved.

1. Introduction

Elastomers belong to a technologically important family of engineering materials. Elastomers or rubbers are widely used in various fields such as automotive industry, building/construction, agriculture, as well as for mechanical engineering applications because of their low modulus, their capability to recover extremely large deformation, and their high internal damping [1–3]. The broad usage of elastomers, in numerous technological applications, created needs for improved properties and distinct performances, such as improved thermal resistance, chemical resistance, environmental stability and conservation of elasticity at low temperature. Rubber specialists are familiar with fillers in industrial scale, since reinforced rubbers with chalk, talk, and carbon black are produced and exploited in commercially available products for more than six decades [4,5].

Rubbers are typical insulating and flexible materials. Nowadays, besides their thermomechanical performance, electrical properties are of significant interest, since dielectric response and conductivity in rubber composites can be tailored by controlling the type, the amount, and

the distribution of inclusions [6,7]. Dispersing of conductive particles, within an insulating phase, affects both electrical polarization and conductance of the composite system.

Acrylonitrile butadiene copolymer (NBR) commercially available since 1930s has been widely used as an oil resistant rubber. However, NBR has been proved susceptible in environmental influences such as ultraviolet light and ozone attack [8]. To overcome this unremunerative performance, chemists hydrogenate NBR targeting to lower the double bond content. The resulting compound, known as hydrogenated acrylonitrile butadiene rubber (HNBR), was commercially introduced in the 1980s as a material suitable for permanent exposure to temperatures ranging from −25 to 150 °C [2]. HNBR addresses advanced requirements of the automotive industry because of its excellent heat and oil resistance properties combined with superior mechanical performance [1]. HNBR is extensively used in applications such as power transmission belts, timing belts, servo-hydraulic hoses, torsion vibration dampers, mounts and seals [1].

HNBR is a polar elastomer wherein its acrylonitrile content may vary [1,8]. The presence of polar nitrile side groups minimizes the interactions with other non-polar chemicals, providing one of the most outstanding features of HNBR, its resistance to non-polar media like oils and fuels. Additionally both mechanical strength and wear resistance of HNBR are enhanced with increasing nitrile concentration.

The temperature range, where an elastomer can be considered as operational, is a crucial factor for choosing the suitable rubber for a specific application. Typically rubbers are used above their glass to rubber transition temperature (T_g). Thus, the lower limit of this operational temperature range is determined by the polymer's glass transition temperature.

Single or multiwall carbon nanotubes (CNTs), when dispersed in a polymer matrix, alter the mechanical and electrical performance of the system [9,10].

In a previous study it has been reported that HNBR/MWCNT nanocomposites further improve, the mechanical properties of HNBR vulcanizates, in tandem with their wear performance [3]. The electrically conductive character of the MWCNTs affects the overall electrical behavior of the nanocomposites, namely their dielectric permittivity and conductivity. The latter offers an additional advantage in applications with moving or rotating parts fabricated with HNBR [11].

Moving or rotating insulating parts progressively accumulate on their surface electrostatic charges, which easily lead to undesirable sparks, causing unexpected and early component's failure. The presence of a conductive leakage current drain could provide a possible solution to the problem. Embedding MWCNTs within HNBR is beneficial to the sample's mechanical performance and at the same time, forms conductive paths inside the composites system, through which leakage current could flow. Furthermore, the presence of conductive inclusions in an insulating medium enhances the electromagnetic interference (EMI) shielding effectiveness of the composite. Dielectric spectroscopy is a powerful experimental method for the investigation of polarization effects, relaxation phenomena, molecular mobility, interfacial effects, conductivity, phase transitions, chemical and thermal events in polymer and polymer matrix composites [5,12]. Dielectric spectroscopy reflects the interaction between matter and electromagnetic waves in a very broad frequency range, monitoring in real time the dynamics of bounded and unbounded charge carriers within complex systems [12–14].

In this work, the morphology and the electrical response of HNBR and MWCNT/HNBR nanocomposites, at two different filler loadings, were studied by means of scanning electron microscopy (SEM), X-ray diffraction (XRD) and broadband dielectric spectroscopy (BDS), respectively.

2. Experimental

2.1. Materials and specimens preparation

Commercially available peroxide curable HNBR (Therban® LT VP/KA 8882 of Lanxess, Leverkusen, Germany) was used for the preparation of the tested specimens. The acrylonitrile content of HNBR was 21%, with Mooney viscosity ML (1 + 4) 100 °C = 74. The composition of the HNBR mix is indicated in Table 1. The curing time of this base mix to reach 90% crosslinking was about 10 min at T = 175 °C. In order to prepare the composite systems, 10 and 20 parts per hundred rubber (phr) per weight MWCNT (Baytubes® C150 P from Bayer Material Science, Leverkusen, Germany) were added to peroxide curable HNBR. MWCNT filled HNBR mixtures were cured at 175 °C for 15 min. Details upon the preparation method can be found elsewhere [3,15].

2.2. Materials characterization

The morphology of the prepared systems was examined by means of SEM at different magnification levels. SEM pictures were taken from cryofractured surface after Au/Pd alloy sputtering using a JEOL JSM-6380LA (Tokyo, Japan) device. The crystallinity of the specimens was deduced from XRD spectra taken with an upgraded in automations Philips PW 1050/25 goniometer and a Cu Kα broad focus X-ray tube (λ = 1.5418 Å). X-ray tube was operated at 40 KV × 30 mA from a Philips PW 11300/00/60 extra stabilized generator. Scanning step was set to 0.1° and all diffractograms have been taken in the range from 10° to 60°.

Thermal transitions were studied by means of differential scanning calorimeter (DSC) by employing a TA Q200 device (TA Instruments, New Castle, USA) operating at a scan rate of 10 °C/min. Samples from each system were placed in an aluminum crucible while an empty one was serving as reference. Temperature was varied from −50 °C to 100 °C.

The electrical response of the systems was assessed by means of BDS using an Alpha-N Frequency Response Analyzer, supplied by Novocontrol Technologies (Hundsagen, Germany). The voltage amplitude (V_{rms}) of the applied field was kept constant at 1000 mV, while frequency varied from 10^{-1} to 10^6 Hz. Isothermal scans were conducted in

Table 1
Composition of peroxide curable HNBR.

Material	Parts
Therban® LT VP/KA 8882 (Lanxess, Leverkusen, Germany)	100
Diphenylamine-based thermostabilizer (Luvomaxx CDPA of Lehmann & Voss, Hamburg, Germany)	1.1
Zinc-containing mercapto-benzimidazole compound (Vulcanox® ZMB 2/C5 of Lanxess)	0.4
t-Butylperoxy-diisopropyl benzene (Perkadox 14-40 B-PD of Akzo-Nobel, Düren, Germany; active peroxide content: 40%)	7.5
MgO	2
Triallyl isocyanurate	1.5
ZnO	2

the temperature range from −100 to 150 °C, in steps of 10 °C. Temperature was controlled via the Quattro system and temperature fluctuations were less than 0.1 °C (Novocontrol Technologies). The employed dielectric test cell was the BDS-1200, parallel-plate capacitor, with two gold-plated electrodes system, supplied also by Novocontrol. Cell was electrically shielded in nitrogen gas atmosphere. The whole experimental setup is fully automated, control and data acquisition were conducted simultaneously via suitable software.

3. Results

Representative SEM images of the cryofractured surface of the HNBR + 20phr MWCNTs specimen are shown in Fig. 1, at three different magnifications. Apparently agglomerates, MWCNTs entanglements and nanodispersion co-exist. However, at the highest magnification (Fig. 1c) a fine dispersion of MWCNTs can be observed.

XRD patterns of all three examined systems are depicted in Fig. 2. The semi-crystalline nature of the HNBR samples under investigation becomes evident from the observed broad peak at $2\theta = 19°$ which is attributed to the long-range stereoregularity of the amorphous state of NBR. Additional sharp peaks in the HNBR diffractograms are observed due to the presence of ZnO and MgO in the composition of HNBR, as well as peaks of Calcite ($CaCO_3$), an ingredient of Perkadox© which is also contained in the composition of HNBR (Table 1). The peaks shown in Fig. 2 at 2θ (degrees) angles of 29.41°, 39.38°, 47.53° and 48.53° are due to calcite, peaks at 31.78°, 34.45°, 36.28°, 47.58° and 56.61° are due to ZnO, while the peak at 43.02° indicates the presence of MgO [16]. Varying crystallinity of HNBR with acrylonitrile content has been reported previously [1,8,17]. The addition of MWCNTs gives rise to an extra rather wide and shallow, graphite like peak (002) located at 25.5°, which is always present in the MWCNTs spectra, as well as in the spectra of different allotropic forms of carbon [18–20]. The degree of HNBR's crystallinity for each system was calculated as the ratio of the area under the peak at 19° to the area under the XRD curve. Obtained values are listed in Table 2. The level of crystallinity for the unfilled HNBR was found to be 30.0%, which is very close to previous reported values with similar acrylonitrile content [17] and appears to increase with the incorporation of MWCNTs. Therefore, MWCNT acted as nucleating agent for the HNBR phase.

The DSC thermographs of all examined materials are depicted in Fig. 3. Recorded traces reveal the glass to
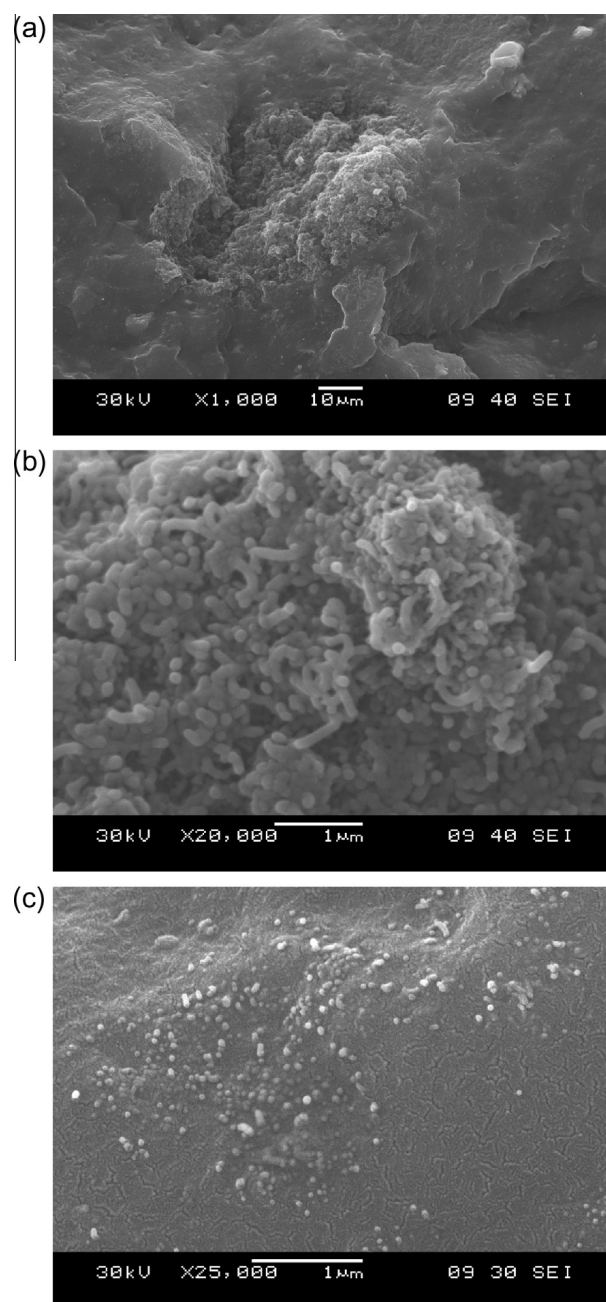

Fig. 1. SEM images from cryofractured surface of the HNBR + 20phr MWCNT specimen at (a) 1000×, (b) 20,000× and (c) 25,000× magnification.
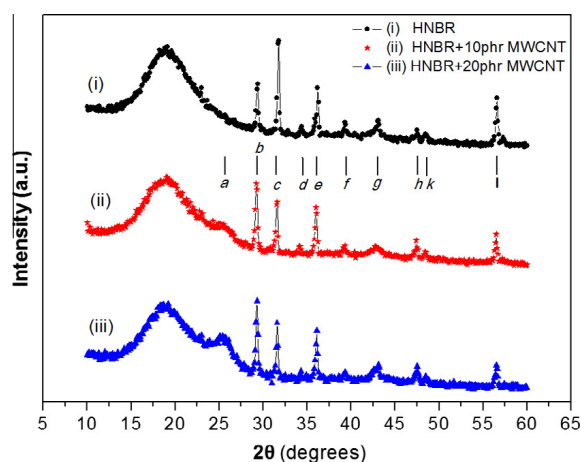
Fig. 2. XRD diffractograms of the (i) HNBR, (ii) HNBR + 10phr MWCNT and (iii) HNBR + 20phr MWCNT systems. Arrow lines indicate peaks positions for a: graphite-like peak, b, f, h, k: calcite, c, d, e, h, l: ZnO and g: MgO peak.

Fig. 3. DSC thermographs of all studied systems.

rubber transition for all three systems at temperatures well below 0 °C. Glass to rubber transition was determined via the midpoint of the transition by employing suitable software supplied by TA. Determined values, listed in Table 2, exhibit a trend to increase with MWCNT content. Besides this transition no other thermal event seems to be present. Thus, at first approximation, DSC traces do not provide support for the existence of HNBR's crystallinity.

The dielectric response of the unfilled HNBR is shown in Fig. 4. Fig. 4a presents the dependence of the real part of dielectric permittivity (ε') upon frequency and temperature. Permittivity attains high values at low frequencies and high temperatures. At this frequency and temperature region permanent and induced dipoles pose sufficient time and energy to align themselves parallel to the applied field approaching maximum polarization of the system. However, the significant high values of (ε') at the lower edge of frequency range and higher edge of temperature range indicate the presence of electrode polarization. Step-like transitions from high to low values of (ε'), at intermediate frequencies, imply the occurrence of relaxation processes. The latter becomes evident in the loss tangent versus frequency and temperature graph in Fig. 4b. Four distinct processes are recorded. At the low frequency and high temperature edge, the observed relaxation is attributed to interfacial polarization (IP) (a phenomenon also known as Maxwell–Wagner–Sillars effect). IP occurs in heterogeneous systems because of the accumulation of unbounded charges at the interface of the constituents. IP is a slow relaxation process (characterized by large relaxation time)
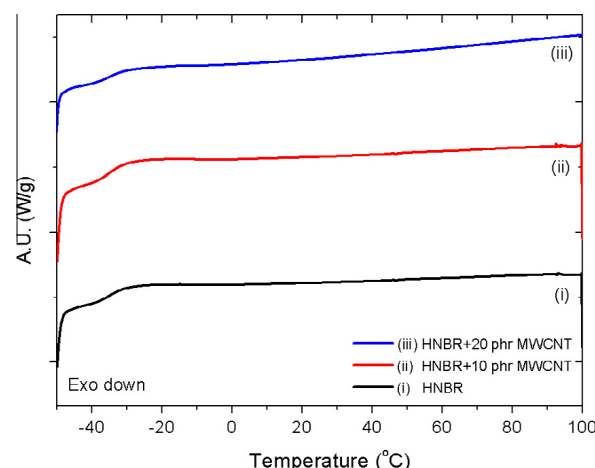
due to the inertia of the formed dipoles to follow the alternation of the applied field. Semi-crystalline polymers and polymers with additives, although unreinforced, exhibit IP between crystalline and amorphous regions [6,7,21–23] or matrix and inserts [24]. Descending relaxation time, the next recorded process is related to the glass to rubber transition of the polymer matrix (α-mode). At temperatures lower than 0 °C two even faster mechanisms are present. The first one occurring in the vicinity of 0 °C is assigned to local motions of polar side groups of the main polymer chain (β-mode). HNBR contains polar side groups of (−CN) which rearrange themselves under the influence of the electric field. Finally, the faster one recorded at the high frequency and low temperature edge is assigned to motions of small parts of the main polymer chain (γ-mode). It is attributed to "crankshaft" motions of the $(CH_2)_n$ units of the HNBR's backbone. The same process has been found to be present in the spectra of other rubbers as well [6,7,23].

The dielectric response of the HNBR + 10phr MWCNT nanocomposite is depicted in Fig. 5, via the three-dimensional graphs of (ε') and ($\tan\delta$) versus frequency and temperature. Both graphs are similar to those of unfilled HNBR and the same four relaxation processes are present. Dielectric spectra of the HNBR + 20phr MWCNT nanocomposite are shown in Fig. 6. The real part of dielectric permittivity (Fig. 6a) attains high values in the low frequency-high temperature range, which diminish rapidly with the increase of frequency. Approximately at 0 °C a step-like transition of (ε') is recorded denoting the existence of a relaxation process. Dielectric loss tangent spectra (Fig. 6b) for the 20phr reinforced nanocomposite deviate from the

Table 2
Values of crystallinity, glass transition temperature, fitting parameters of Eq. (3), and activation energy of all studied systems.

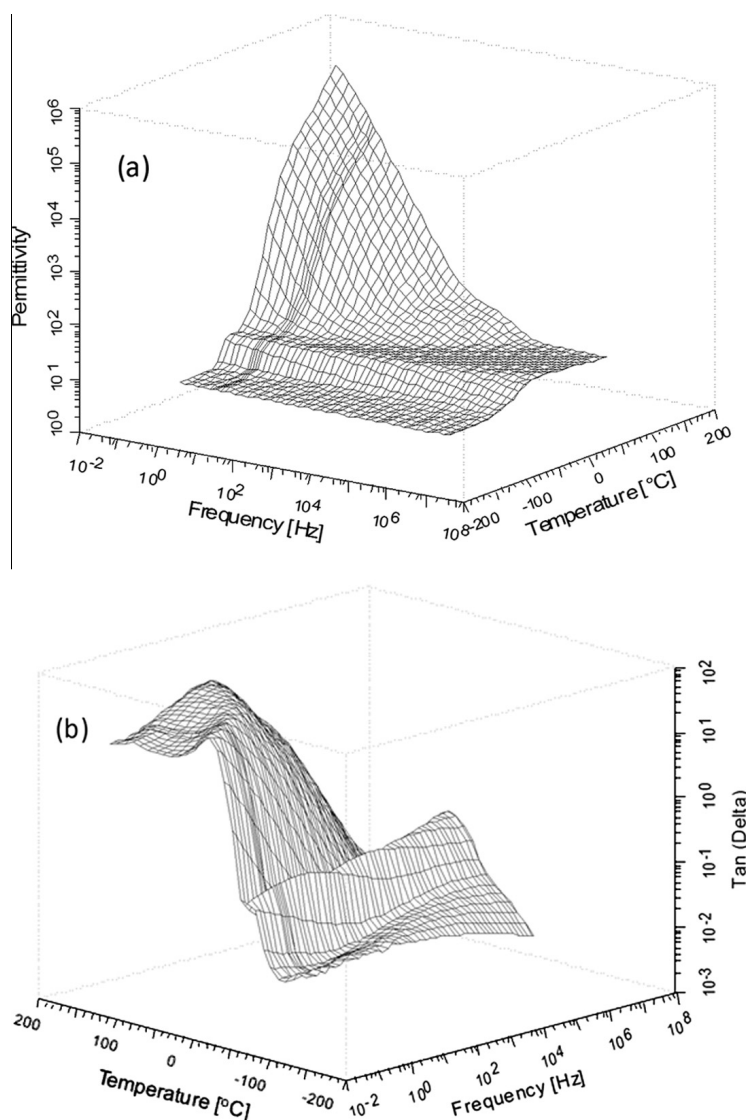| System	Crystallinity (%)	Glass transition temperature (°C)	α-Relaxation		β-Relaxation	γ-Relaxation
			A	T_0 (K)	Activation energy (eV)	
HNBR	30.0	−38.3	13.2	159.4	1.91	0.44
HNBR + 10phr MWCNT	35.8	−35.5	0.33	266.1	2.21	0.30
HNBR + 20phr MWCNT	47.6	−34.8	–	–	–	–

MACROMOLECULAR NANOTECHNOLOGY

Fig. 4. Variation of (a) real part of permittivity and (b) loss tangent, with temperature and frequency for unfilled HNBR.

corresponding response of the two other examined systems. The only clearly formed loss peak is the one in the vicinity of 0 °C, which, as already mentioned, is ascribed to the local rearrangement of the polar cyano groups. Additionally, a broad loss peak seems to be formed in the low frequency and high temperature range. The latter could be the result of superposition of α-mode and IP. From Fig. 6b no evidence for γ-mode can be detected.

4. Discussion

Glass transition temperature and crystallinity of HNBR have been found to vary with the acrylonitrile content, although DSC curves do not always, markedly, reveal the existence of crystalline regions [1,8]. In our case acrylonitrile content was constant at 21%. Melting of crystalline regions is detected as endothermic processes in DSC curves via the formation of peaks or humps at temperatures higher than glass to rubber transition temperature (T_g) and be-

low 100 °C [1,8]. Rubbers with high acrylonitrile level exhibit two melting peaks and their crystallinity is attributed to alternating acrylonitrile–ethylene sequences [1]. At lower acrylonitrile content, as in our case, crystallization of longer methylene sequences occurs along the HNBR polymer backbone. The latter becomes evident via the formation of endothermic humps or shoulders right afterwards the glass to rubber transition zone [1,17]. Observing the DSC traces in Fig. 3, one can distinguish the presence of such humps in all studied systems. Under this point of view, thermographs provide secondary support to XRD results.

In this study dielectric data have been analyzed by means of dielectric permittivity and electric modulus formalism. Electric modulus is defined as the inverse quantity of complex dielectric permittivity, via Eq. (1):

$$M^* = \frac{1}{\varepsilon^*} = \frac{\varepsilon'}{\varepsilon'^2 + \varepsilon''^2} + j\frac{\varepsilon''}{\varepsilon'^2 + \varepsilon''^2} = M' + jM'' \tag{1}$$
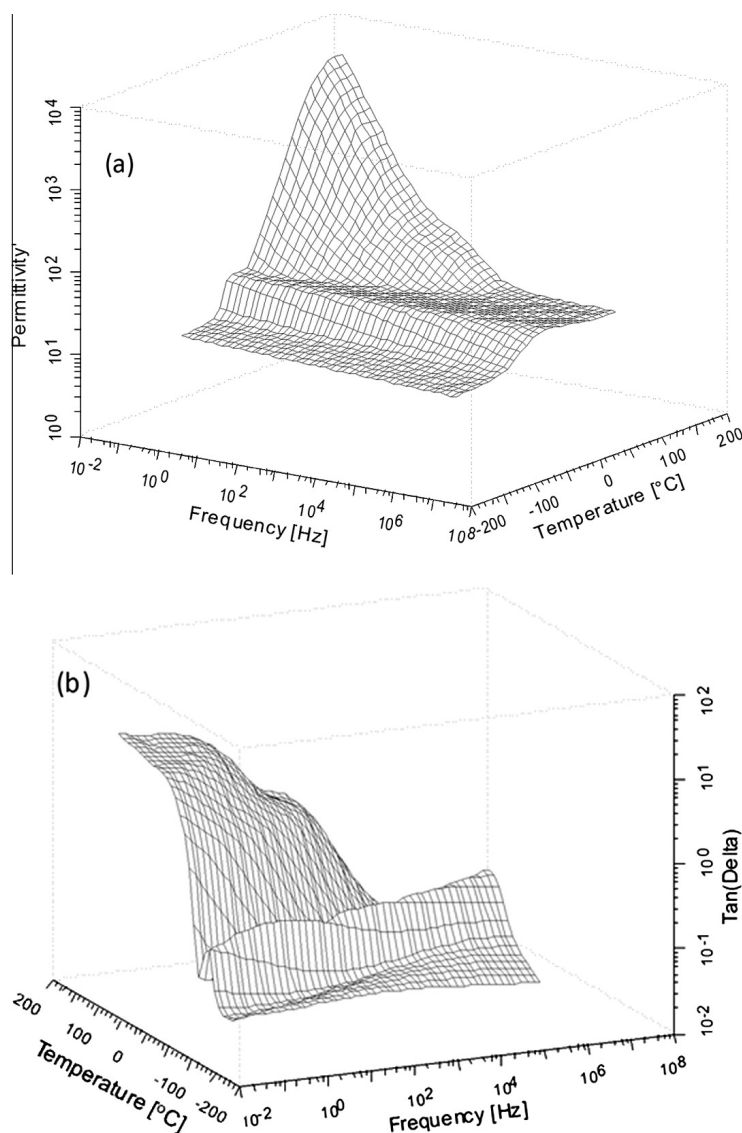
Fig. 5. Variation of (a) real part of permittivity and (b) loss tangent, with temperature and frequency for the HNBR + 10phr MWCNT system.

where ε', M' are the real and ε'', M'' the imaginary parts of dielectric permittivity and electric modulus, respectively. Electric modulus formalism has been proved very efficient for analyzing dielectric data of polymer matrix nanocomposites [6,7,25–27]. Fig. 7 presents the variation of loss modulus index (M'') as a function of temperature at two different frequencies (a) 10 Hz and (b) 1 MHz. In Fig. 7a the relatively slow relaxation processes are detected in the spectra of HNBR and HNBR + 10phr MWCNTs. These processes are glass to rubber transition (α-mode) and IP. Both systems exhibit an α-relaxation loss peak located at −30 °C, a temperature close to the T_g value determined via DSC. Small deviations in values of T_g determined via different experimental techniques, should be attributed to the dynamic nature of the phenomenon. At higher temperatures the IP loss peak is recorded for both systems. It is important to point out the differences of IP between these two systems. IP in HNBR results from the accumulation of unbounded charges at the interfaces between crystalline

and amorphous regions, leading to a symmetrical narrow peak approximately at 17 °C. On the other hand, the corresponding peak of the HNBR + 10phr MWCNT specimen, is broader, recorded at higher temperature (approximately at 42 °C) and is characterized by lower ordinate. In this composite besides the crystalline/amorphous regions interface an additional interfacial component exists. This is the interface between HNBR and MWCNTs. The addition of MWCNTs increases the conductivity of the system and at the same time the electrical heterogeneity of their constituents. Enhanced heterogeneity alters the intensity of the IP effect, which can be realized via the high values of real and imaginary part of dielectric permittivity. Recalling Eq. (1), in the electric modulus presentation, the increase of intensity of IP is demonstrated by reduced values of M' and M''. Thus, the lower values of loss modulus index (M'') can be considered as a strong indication for the existence of intensive interfacial phenomena. The broadness of the peak can be assigned to interactions between the constituents of the
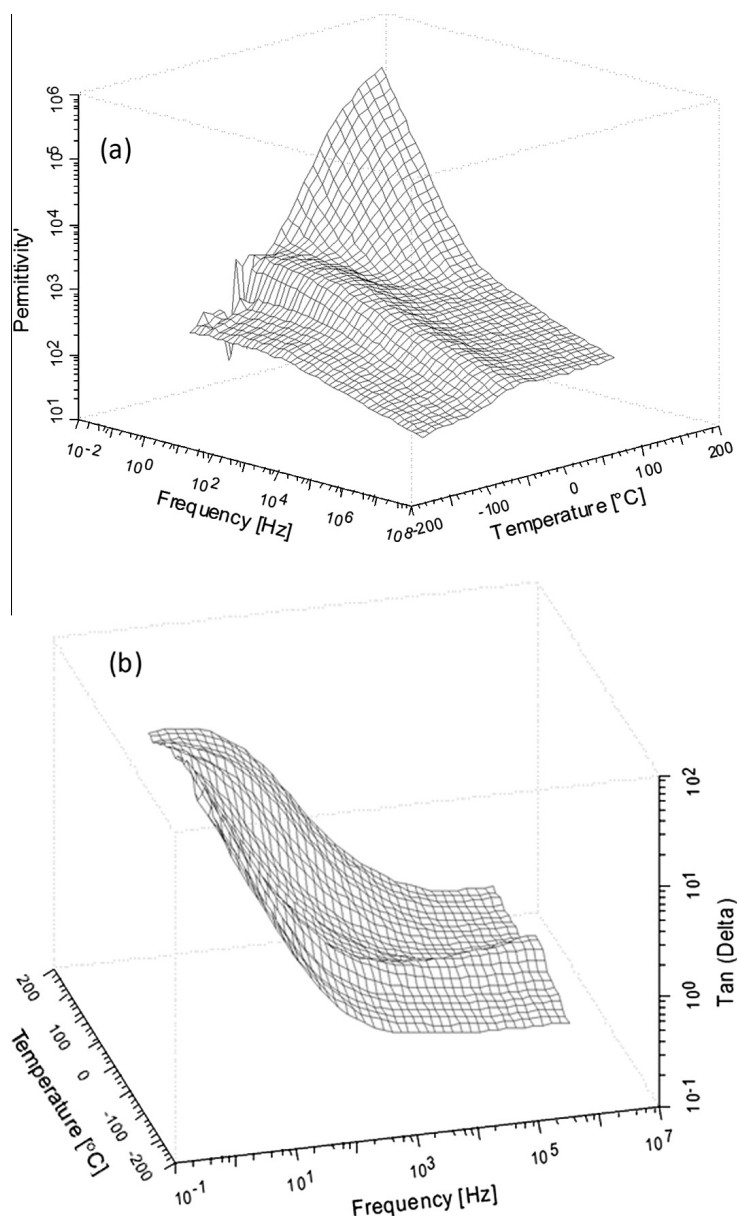
Fig. 6. Variation of (a) real part of permittivity and (b) loss tangent, with temperature and frequency for the HNBR + 20phr MWCNT system.

nanocomposite. Interfaces with varying geometrical characteristics contribute to interfacial relaxation phenomena with different dynamics or relaxation times, the superposition of all interfacial effects results in the recorded broad peak. Furthermore, shifting of the loss peak position to higher temperature implies an increase of relaxation time and an increase of the activation energy of the process with the addition of 10phr MWCNTs. An analogous behavior for IP has been reported in polyurethane rubber/layered silicates nanocomposites [6]. The spectrum of HNBR + 20phr MWCNTs composite deviates remarkably from the spectra of the other two systems. M'' attains very low values, and no relaxation process can be detected. This behavior is in accordance with the results of Fig. 6, and the very high values of real and imaginary part of dielectric permittivity. This further suppression of M'' values is related to the accessional increase of conductivity. Increasing the con-

ductive phase content in a binary system with insulating matrix, alters the overall conductivity of the composite and at a critical concentration, known as percolation threshold, a dramatic increase of conductivity occurs [20,28–30]. At concentrations close to the critical one, charges are able to migrate at larger distances within the composite because of the formation of conductive paths. Charges accumulated at the system's interfaces are now able to migrate contributing to the increase of conductivity and at the same time diminish or even eliminate IP process [30]. On the other hand, the absence of even a small loss peak related to the glass to rubber transition is peculiar. It might be resulted from the reduction of the amorphous areas, which are now constrained between extensive rigid crystalline regions. Their relaxation is thus hindered, and the dynamics of the process is delayed. The broad peak in Fig. 6b is in good agreement with the previous assumption,
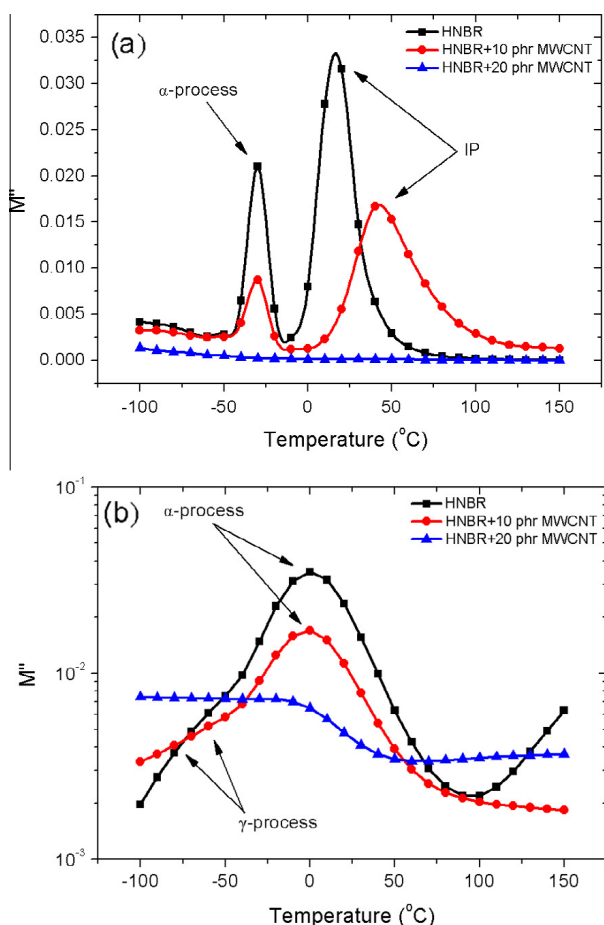
Fig. 7. Variation of modulus loss index with temperature for all studied systems at (a) 10 Hz and (b) 1 MHz.

and the DSC results which revealed an increasing trend of T_g with the crystallinity of the systems. The increase of T_g with MWCNT content should be attributed to the enhanced restrictions imposed to the macromolecules in the amorphous parts by the crystalline regions.

On the contrary to Fig. 7a, fast relaxation processes are depicted in Fig. 7b, where the variation of the imaginary part of electric modulus versus temperature at 1 MHz is presented. β-relaxation is clearly detected via the loss peak in the vicinity of 0 °C for both HNBR and HNBR + 10phr MWCNT systems, while γ-mode is recorded as a hump at the left side of the peak in the temperature range from −100 °C to −40 °C. Both processes are present in the spectrum of the HNBR + 20phr MWCNT nanocomposite. Their superposition forms a plateau at lower temperatures, which follows a step like transition to lower values of M'' at temperatures higher than 0 °C. The relaxation mechanisms shown in Fig. 7a (α-relaxation and IP), have been shifted to higher temperatures (out of the experimental "window") because of the temperature–frequency superposition.

Conductivity measurements for all three tested systems at various frequencies, as a function of reciprocal temperature are depicted in Fig. 8. Conductivity rises with conductive filler content, and especially for the HNBR + 20phr MWCNT nanocomposite, this alteration ranges from 3 to

6 orders of magnitude at high and low temperature edges respectively. In the low temperature region (temperatures lower than −50 °C), in all examined systems, conductivity tends to acquire constant values. Conductivity increases with the frequency of the applied field, and at high temperatures conductivity values are converging, especially in the case of HNBR (Fig. 8a). The resulting form of the $\sigma_{ac} = f(1/T)$ curves, strongly deviates from a pure Arrhenius behavior,
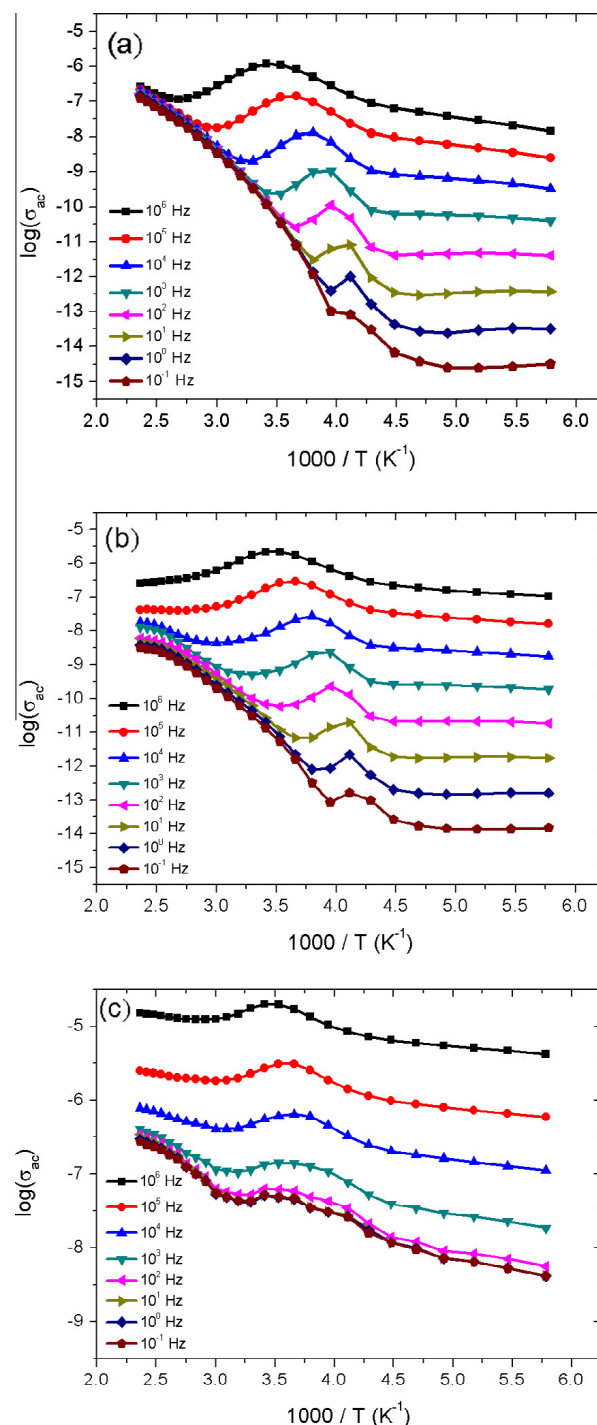

Fig. 8. Conductivity as a function of reciprocal temperature at various frequencies for (a) HNBR, (b) HNBR + 10phr MWCNT and (c) HNBR + 20phr MWCNT systems.

MACROMOLECULAR NANOTECHNOLOGY

signifying that the occurring conductance mechanisms do not correspond to a single thermally activated process and cannot be described via a single exponential relationship. Thus, at temperatures higher than −50 °C conductivity's activation energy depends on frequency and temperature and it is reasonable to assume that a range of activation energies is involved. Furthermore, the spread of conductivity values with temperature increases as the frequency of the applied field diminishes. At low frequencies charge carriers are forced to drift over large distances addressing high energy barriers because of the insulating matrix. Increase of temperature facilitates this migration by offering additional thermal excitation. When frequency rises charge carriers' mean displacement is significantly reduced. Charges are now addressing lower energy barriers and are able to jump between adjacent conductive sites, altering thus the overall measured conductivity. In the unreinforced HNBR conductivity values exhibit remarkable proximity, at high temperatures, being independent from the frequency of the applied field. The presence of MWCNTs in the nanocomposite systems increases the number of conductive sites and charge carriers density, and as a consequence conductivity increases, (Fig. 8b,c). The influence of frequency seems to become stronger than that of temperature with increasing MWCNT content. The latter could be considered as an indirect indication for energy barriers reduction. In an intermediate temperature range (between −30 °C and 20 °C), a peak is formed in all studied systems. This peak is related to the glass to rubber transition of the amorphous regions, and it corresponds to the systems' T_g. Accordingly peak shifts to higher temperatures with increasing frequency. Glass transition temperatures as determined via DSC, or resulted from the loss peak position in the dielectric spectra, lie within the range mentioned previously.

Relaxation dynamics or peak loss shift rate with temperature for the HNBR and HNBR + 10phr MWCNT systems is presented in Fig. 9. The temperature dependence of loss peak position for β- and γ-relaxations follows an Arrhenius type behavior and can be described via Eq. (2):

$$f_{\max} = f_0 \exp\left(-\frac{E_A}{k_B T}\right) \qquad (2)$$

where E_A is the activation energy of the process, f_0 pre-exponential factor, k_B the Boltzmann constant and T the absolute temperature.

On the other hand, peak shift rate for α-relaxation is not constant and is described via the Vogel–Fulcher–Tamann (VFT) equation, which is expressed by Eq. (3):

$$f_{\max} = f_0 \exp\left(-\frac{A T_0}{T - T_0}\right) \qquad (3)$$

where f_0 is a pre-exponential factor, A a constant being the measure of activation energy, T_0 the Vogel temperature or ideal glass transition temperature, and T the absolute temperature. According to VFT equation, relaxation rate increases rapidly at lower temperatures because of the reduction of free volume. Calculated values of activation energy via fitting experimental data for β- and γ-relaxations via Eq. (2), as well as fitting parameters for α-relax-
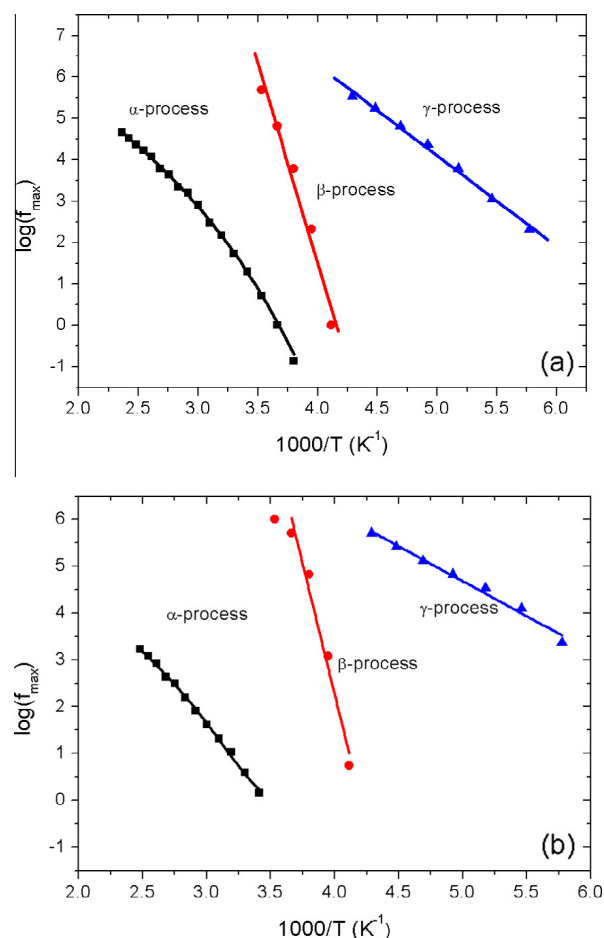

Fig. 9. Loss peak position, of the recorded relaxations, as a function of reciprocal temperature for (a) HNBR and (b) HNBR + 10phr MWCNT systems.

ation determined by employing Eq. (3), are listed in Table 2.

The absence of clearly formed peaks in the case of the HNBR + 20phr MWCNT nanocomposite prohibits the evaluation of the relaxation dynamics parameters in this system. Moreover, the limited number of peak points for the IP relaxation, located at the low frequency and high temperature edge, resulted in low reliability fittings, and thus are omitted from Fig. 9a and b. Determined values of activation energy via Eq. (2) of β- and γ-processes as well as fitting parameters of Eq. (3) for α-process are also listed in Table 2. Polar side groups' rearrangement seems to be restricted from crystalline regions, since the activation energy of this process appears elevated (~2 eV) and tends to increase further with crystallinity level. On the other hand activation energy for γ-relaxation remains low and decreases with crystallinity.

5. Conclusions

Morphology, thermal response, dielectric properties and electrical conductivity of HNBR and MWCNT reinforced HNBR systems were studied. XRD spectra revealed the presence of crystalline regions in HNBR which further

increases with the addition of MWCNTs. Glass to rubber transition, as determined via DSC, was found to lie in the range from −38 to −34 °C. Dielectric permittivity increases with diminishing frequency and increasing temperature. Loss spectra revealed the presence of four relaxation processes, which with descending relaxation time, were attributed to IP, glass to rubber transition of amorphous regions of HNBR (α-relaxation), local motions of polar side cyano groups (β-relaxation), and to "crankshaft" motions of the $(CH_2)_n$ units of the HNBR's backbone (γ-relaxation). IP relaxation process is attributed to the accumulation of charges at the interface between amorphous and crystalline regions, as well as between HNBR and MWCNTs. Conductivity increases with MWCNT content, frequency and temperature. The influence of temperature is more pronounced in the case of the unfilled HNBR. Below −50 °C conductivity values appear to be temperature independent for all studied systems. Finally, relaxation dynamics are affected by the systems' level of crystallinity.

References

[1] Wrana C, Reinartz K, Winkelbach HR. Therban®- the high performance elastomer for the new millennium. Macromol Mater Eng 2001;286:657–62.

[2] Wang XP, Huang A-M, Jia D-M, Li Y-M. From exfoliation to intercalation-changes in morphology of HNBR/organoclay nanocomposites. Eur Polym J 2008;44:2784–9.

[3] Felhös D, Karger-Kocsis J, Xu D. Tribological testing of peroxide cured HNBR with different MWCNT and silica contents under dry sliding and rolling conditions against steel. J Appl Polym Sci 2008;108:2840–51.

[4] Karger-Kocsis J, Wu C-M. Thermoset rubber/layered silicate nanocomposite. Status and future trends. Polym Eng Sci 2004;44:1083–93.

[5] Psarras GC, Gatos KG. Relaxation phenomena in elastomeric nanocomposites. In: Mittal V, Kim JK, Pal K, editors. Recent advances in elastomeric nanocomposites. Berlin-Heidelberg: Springer-Verlag; 2011. p. 89–118. ISBN: 978-3-642-15786-8.

[6] Psarras GC, Gatos KG, Karahaliou PK, Georga SN, Krontiras CA, Karger-Kocsis J. Relaxation phenomena in rubber/layered silicate nanocomposites. Exp. Polym Lett 2007;1:837–45.

[7] Siengchin S, Karger-Kocsis J, Psarras GC, Thomann R. Polyoxymethylene/polyurethane/alumina ternary composites: structure, mechanical, thermal and dielectrical properties. J Appl Polym Sci 2008;110:1613–23.

[8] Severe G, White JL. Physical properties and blend miscibility of hydrogenated acrylonitrile–butadiene rubber. J Appl Polym Sci 2000;78:1521–9.

[9] Dang Z-M, Yao S-H, Yu H-P. Effect of tensile strain on morphology and dielectric property in nanotube/polymer nanocomposites. Appl Phys Lett 2007;90:012907.

[10] Jiang M-J, Dang Z-M, Yao S-H, Bai J. Effects of surface modification of carbon nanotubes on the microstructure and electrical properties of carbon nanotubes/rubber nanocomposites. Chem Phys Lett 2008;457:352–6.

[11] Sofos G. Electrical response of HNBR and composite rubber blends of HNBR/FKM which incorporate MWCNTs, MSc Thesis University of Patras, Patras, Greece; 2009.

[12] Psarras GC. Conductivity and dielectric characterization of polymer nanocomposites. In: Tjong SC, Mai Y-M, editors. Polymer nanocomposites: physical properties and applications. Cambridge: Woodhead Publishing Limited; 2010. p. 31–69.

[13] Kremer F, Schönhals A. Analysis of dielectric spectra. In: Kremer F, Schönhals A, editors. Broadband dielectric spectroscopy. Berlin: Spinger; 2003. p. 35–98.

[14] Vassilikou-Dova A, Kalogeras M. Dielectric analysis (DEA). In: Menczel JD, Prime RB, editors. Thermal analysis of polymers, fundamentals and applications. New Jersey: Wiley; 2009. p. 497–614.

[15] Xu D, Karger-Kocsis J, Major Z, Thomann R. Unlubricated rolling wear of HNBR/FKM/MWCNT compounds against steel. J Appl Polym Sci 2009;112:1461–70.

[16] Downs RT, Hall-Wallace M. The american mineralogist crystal structure database. Am Mineral 2003;88:247–50.

[17] Bieliński DM, Ślusarski L, Wlochowicz A, Ślusarczyk C. Structure and mechanical properties of nitrile rubbers modified with iodine. J Appl Polym Sci 1998;67:501–12.

[18] Cao A, Xu C, Liang Ji, Wu D, Wei B. X-ray diffraction characterization on the alignment degree of carbon nanotubes. Chem Phys Lett 2001;344:13–7.

[19] Li W, Liang C, Zhou W, Qiu J, Zhou Z, Sun G, et al. Preparation and characterization of multiwalled carbon nanotube-supported platinum for cathode catalysts of direct methanol fuel cells. J Phys Chem B 2003;107:6292–9.

[20] Psarras GC. Charge transport properties in carbon black/polymer composites. J Polym Sci Part B: Polym Phys 2007;45:2535–45.

[21] Pissis P, Kanapitsas A, Savelyev YV, Akhranovich ER, Privalko EG. Influence of chain extenders and chain end groups on properties of segmented polyurethanes. II. Dielectric study. Polymer 1998;39:3431–5.

[22] Korzhenko A, Tabellout M, Emery JR. Influence of a metal–polymer interfacial interaction on dielectric relaxation properties of polyurethane. Polymer 1999;40:7187–95.

[23] Kalini A, Gatos KG, Karahaliou PK, Georga SN, Krontiras CA, Psarras GC. Probing the dielectric response of polyurethane/alumina nanocomposites. J Polym Sci Part B: Polym Phys 2010;48:2346–54.

[24] Patsidis AC, Kalaitzidou K, Psarras GC. Dielectric response, functionality and energy storage in epoxy nanocomposites: barium titanate vs exfoliated graphite nanoplatelets. Mater Chem Phys 2012;135:798–805.

[25] Salvetat JP, Bhattacharyya S, Pipes RB. Progress on mechanics of carbon nanotubes and derived materials. J Nanosci Nanotechnol 2006;6:1857–82.

[26] Chanmal CV, Jog JP. Dielectric relaxations in PVDF/BaTiO$_3$ nanocomposites. Exp Polym Lett 2008;2:294–301.

[27] Tantis I, Psarras GC, Tasis D. Functionalized graphene-poly(vinyl alcohol) nanocomposites: physical and dielectric properties. Exp Polym Lett 2012;6:283–92.

[28] Psarras GC. Conduction processes in percolative epoxy resin/silver particles composites. Sci Adv Mater 2009;1:101–6.

[29] Shrivastava NK, Maiti S, Suin S, Khatua BB. Influence of selective dispersion of MWCNT on electrical percolation of *in-situ* polymerized high-impact polystyrene/MWCNT nanocomposites. Exp Polym Lett 2014;8:15–29.

[30] Pontikopoulos PL, Psarras GC. Dynamic percolation and dielectric response in multiwall carbon nanotubes/poly(ethylene oxide) composites. Sci Adv Mater 2013;5:14–20.

MACROMOLECULAR NANOTECHNOLOGY